Check for updates

ADVANCED MATERIALS TECHNOLOGIES
www.advmattechnol.de

Green Light Vat-Photopolymerisation for 3D Printing Hydrogels with Complex Lattice Structures

Livia M. Kalossaka, Ali A. Mohammed, Laura Bastos, Laura M. C. Barter, and Connor W. Myant*

Moving beyond UV curing systems opens new potential application spaces such as biological, portable printing solutions, as well as innovative chemistries and material properties. A novel visible light printer is proposed for the first time using green Digital Light Processing (gDLP) at a wavelength of 514 nm. Green LED lights are integrated into a commercial desktop DLP printer to 3D print hydrogels with complex designs at high resolution. A workflow process is presented to develop and optimize formulations for gDLP, resulting in two novel in-house photoresin formulations made specifically for green light printing. These formulations comprise $PEGDA_{700}$ with and without acrylamide, using a type II photoinitiating system of Eosin Y, triethylamine, and N-vinylpyrrolidone. The photoresins are optimized to achieve highly vascularized lattice prints by modulating layer light exposure, chemical components, and photoinitiator concentrations. The gDLP successfully printed hydrogels with a layer height of 50 µm and feature dimensions as small as 0.3 mm by adjusting light duration per layer. 3D printed hydrogels using both formulations are tested for varying design complexity, including ISO/ASTM standards, and evaluated with optical imaging, SEM, and mechanical testing. This study highlights gDLP technology's potential for diverse applications in tissue engineering and sustainable materials.

1. Introduction

The development of additive manufacturing (AM) techniques has had an enormous impact on materials development in the last 30 years.[1] However, the technology has not reached its full potential due to the restricted functionality of the structures fabricated often limited to material selection and their related printing technologies.[2] An area of research that has attracted attention due to its vast range of applications is 3D printing of hydrogels.[3] Hydrogels are 3D crosslinked polymer networks that can hold large amounts of water. Their hydrophilic nature renders them ideal for many applications[4,5] as they can mimic the water content and diffusion of solutes present in natural environments.

Additive Manufacturing (AM) has gained traction for fabricating structures with novel properties. These include biomimetic scaffolds that mimic natural tissues, hydrogels compatible with both mammalian cells (cytocompatible) and plants (phytocompatible), as well as dynamic living materials.[6–9] This method is recognized as a cost-effective, precise, and rapid solution for creating 3D structures suitable for hosting living organisms.[10] For example, 3D bioprinting has emerged as a research focus, allowing the construction of biomimetic scaffolds in a single step. These scaffolds feature well-controlled architectures designed to mimic biological characteristics.[6,7] Recently, applications for microorganism-powered living materials

L. M. Kalossaka, A. A. Mohammed, L. Bastos, C. W. Myant
Dyson School of Design Engineering
Imperial College London
South Kensington Campus
London SW7 2AZ, UK
E-mail: livia.kalossaka@imperial.ac.uk

L. M. Kalossaka, L. M. C. Barter
Department of Chemistry
Molecular Sciences Research Hub
Imperial College London
82 Wood Lane, London W12 0BZ, UK

The ORCID identification number(s) for the author(s) of this article can be found under https://doi.org/10.1002/admt.202500090

© 2025 The Author(s). Advanced Materials Technologies published by Wiley-VCH GmbH. This is an open access article under the terms of the Creative Commons Attribution License, which permits use, distribution and reproduction in any medium, provided the original work is properly cited.

DOI: 10.1002/admt.202500090

L. M. Kalossaka
Department of Life Sciences Imperial College London
South Kensington Campus
London SW7 2AZ, UK

A. A. Mohammed
School of Design
Royal College of Art
1 Hester Rd, London SW11 4AY, UK

L. M. C. Barter
Institute of Chemical Biology
Molecular Sciences Research Hub
Imperial College London
82 Wood Lane, London W12 0BZ, UK

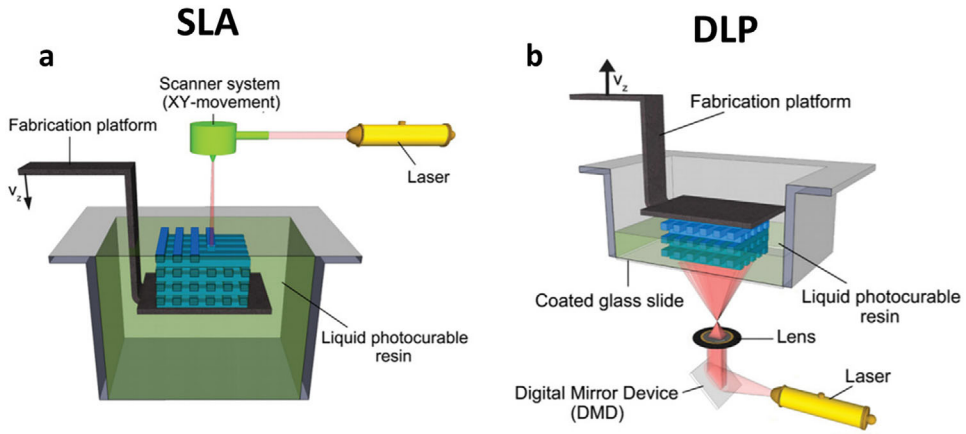


Figure 1. a) Scheme of top-down stereolithography (SLA) and (b) bottom-up digital light processing (DLP). Vz represents platform movement in the z-direction. Reproduced with permission.[23]

have also emerged which could be used for on-demand chemical manufacturing, environmental remediation as well as sensing devices.[11]

With regards to methods used for 3D printing hydrogels, the most common types of technologies used are: Material jetting (MJT), Material extrusion deposition (MEX) and Vat-Photopolymerisation (VPP).[12]

Each technique is associated with a biofabrication window that dictates the ideal characteristics of the material to be processed for the fabrication of high shape fidelity hydrogels suited to support cell functions.[13,14] Furthermore, each printing technology requires specific hydrogel formulations to undergo physical and/or chemical crosslinking.[15] Often, in MEX these materials face challenges related to both high resolution and mechanical strength.[16] This is primarily due to the necessity of using low viscosity inks, which, in turn limits the possibility to print features that can accurately replicate the properties of natural tissues (e.g., porosity).[17] Additionally, the shear stress applied to cells during the extrusion process tends to limit cell viability.[18] While 3D printing for biological applications has garnered significant attention, it continues to face technical challenges, particularly in constructing scaffolds with μm resolution and sufficient mechanical strength to support the growth of living organisms.

To address these challenges, VPP stands out as a promising technique for hydrogel manufacturing. Unlike other methods, VPP does not apply direct force to cells during printing, which preserves a high level of cell viability.[19] Furthermore, it leverages light as a means to regulate chemical reactions, akin to nature's photosynthesis process.[20] Despite VPP's considerable advantages in terms of resolution, shape complexity and speed (e.g., volumetric 3D printing and LCD printing),[21] its application for living organisms and evolutionary advancements is constrained by the use of limited photoresins, including photoinitiators and photopolymers, which often exhibit high irritancy levels or even cytotoxicity in their uncured state.[22] Two main types of light regulators exist for VPP: those which use a laser (e.g., SLA) or a projector (e.g., DLP) as shown in **Figure 1**.

In SLA the laser beam moves independently curing raster lines with the resolution being delimited by the laser spot size. Instead, DLP typically uses a projector screen that will project the layers of squared pixels in the photoresin. Hence the limiting factor here is the size of the pixels of the projector screen. In this research, a subgroup of DLP based printer is investigated, LCD (liquid crystal display) which uses an LCD screen instead of a projector to illuminate one entire layer of the image.[24] An advantage of using an LCD, is that the light source array can be expanded by adding more emitter units, without reducing the intensity per unit surface area, and thereby enabling the same per-layer exposure time at virtually any size for which a liquid crystal film mask can be manufactured. Currently UV-based systems present several drawbacks such as: i) inducing cytotoxicity, ii) utilizing UV photons with limited penetration depth, restricting the achievable layer thickness of the printed material, iii) Prolonged exposure to high-energy UV light leading to the formation of unwanted side reactions involving both the reactants and products.[22] Recent advances in vat photopolymerization have explored green, red, and near-infrared light systems to reduce phototoxicity and improve penetration depth.[25–27] However, many NIR-based approaches face challenges such as limited water solubility of photoinitiators and potential cytotoxicity from electron-transfer catalysts.[28] In contrast, our green-light DLP system employs commercially available 514 nm LEDs which enable reduced cost and safer operating conditions due to their modularity and widespread accessibility.[29] Combined with a continuous vat recoating process, this systems achieves sub-300 μm resolution without complex resin replenishment. Additionally, using higher molecular weight PEGDA compared to previous studies using green light,[25] enhances hydrogel mechanical stability and biocompatibility. However, green-light-mediated polymerization may require the development of specialized photoinitiator systems with strong absorption in the visible spectrum, as many conventional initiators are optimized for UV activation. These should exhibit good excitation under green light, high quantum yields, low energy activation, and high water-dispersion.[30] Additionally, while the lower energy of green photons reduces unwanted side reactions, it may also slow polymerisation kinetics necessitating longer exposure times or higher light intensities to achieve sufficient crosslinking; a trade-off that remains manageable in applications prioritizing biocompatibility over speed. Despite these considerations, the shift towards green-light

© 2025 The Author(s). Advanced Materials Technologies published by Wiley-VCH GmbH

2365709x, 2025, 19, Downloaded from https://advanced.onlinelibrary.wiley.com/doi/10.1002/admt.202500090 by Imperial College London, Wiley Online Library on [03/11/2025]. See the Terms and Conditions (https://onlinelibrary.wiley.com/terms-and-conditions) on Wiley Online Library for rules of use; OA articles are governed by the applicable Creative Commons License

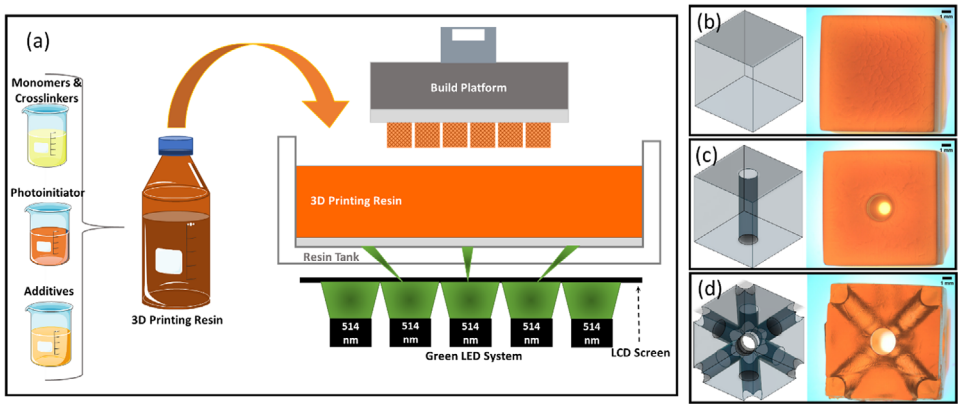


Figure 2. a) Schematic showing a green digital light processing (gDLP) printer, on the right displaying a comparison between CAD designs and 3D printed models of (b) 1 cm^3 Solid, (c) 1 cm^3 single central channel (Hole) and (d) 1 cm ∗ 3 single unit 7-strut lattice cube (Lattice) using the $gDLP_{PEGDA/AA}$ formulation. Scale bar represents 1 mm.

vat photopolymerisation represent a promising paradigm for advancing additive manufacturing, especially in biomedical, (bio)electronic and soft-material applications where safety, deeper light penetration, and compatibility with biological entities (e.g., cells, proteins) take precedence over fast curing times.

Here we demonstrate a green light initiation system with validation on controlling material properties within our novel formulation space. The design process is aimed at increasing biological viability whilst maintaining high-resolution printing and employing more widely available materials. We therefore introduce a visible light-based photoinitiator (PI) setup employing cost-effective, water-soluble components to create hydrogel structures with intricate internal architectures, employing a customized commercial LCD printer (Photocentric Ltd, UK) equipped with green LEDs (514 nm). Consequently, this study fulfills the demand for innovative photocurable 3D printing methodologies and photoresins capable of rapidly producing intricate, high-resolution constructs.[31] Employing water as a solvent and devising a visible light photoinitiator system addresses concerns regarding toxicity and facilitates the fabrication of biomimetic environments. Despite challenges associated with water, such as diffusion limitations, our approach paves the way for new integrated biofabrication techniques. The main monomers used for light-based polymerisation have been selected based on their mechanical, biocompatible and photocurable properties. The most reported ones are poly(ethylene glycol) diacrylate (PEGDA), naturally-derived gelatin methacrylate (GelMA) and hyaluronic acid (HA).[10] Of these, PEGDA represents a strong first choice for initial trials due to its availability, affordability, biocompatibility and tunable mechanical properties.[32]

2. Experimental Section

2.1. Materials

Compounds were purchased from the following manufacturers and used directly without additional purification: $PEGDA_{700}$ (polyethylene glycol diacrylate, average MW 700, stabilized with 100 ppm MEHQ and 300 ppm BHT; Sigma Aldrich), acrylamide (AAm, 99% Sigma-Aldrich), Eosin Y (99% Sigma Aldrich), triethanolamine (TEA, 99.5% Sigma Aldrich), and 1-vinyl-2 pyrrolidinone (NVP, 98% Merck). Distilled water (DI) was used as the solvent for all formulations. The solutions were prepared in darkness due to the presence of light sensitive compounds. They were then stored in amber vials to block ambient UV/visible light, preventing unintended activation of the photoinitiator system and stored in a fridge at 6° C to reduce the rate of the MEHQ inhibitor consumption (to stabilize acrylate monomers) and used within 7 days.

2.2. Green Light Digital Light Processing (gDLP) Printer

A commercially available LCD 3D printer (LC Precision 1.5, Photocentric ltd) was modified by replacing the 405 nm UV LEDs with 514 nm green light LEDs, here named gDLP. To achieve this, the printer was disassembled to reach the hardware components and introduce the new set of LEDs. To absorb and dissipate the heat generated by the electronic components, a heatsink was installed to secure safe operation for successive hours of printing. The projector LCD resolution is 2160 × 1440 pixels. Each pixel being 47.25 µm × 47.25 µm at the image plane. The minimum achievable layer thickness is 10 µm. However, the recommended layer height is 25 µm. The machine power density is 10 mW/cm^2. Each LED contains a 4 mm^2 emission surface area and a maximum current up to 0.7 A. The full width at half maximum (FWHM) of each LED is 15°. The maximum build plane for the printer in its current configuration is 68.04 mm x 120.96 mm. The materials and methods used are reported in the Appendix.

The CAD files were uploaded to the Photocentric printing software (Photocentric Studio). The STL files were then sliced using Photocentric Studio to create a CWS file and uploaded to the printer via a USB.

2.3. Optical Imaging

Freshly prepared samples were imaged using a UltraZOOM-3 GX Optical Microscope to examine the print dimensions relative to their respective CAD designs, preceding the swelling studies.

© 2025 The Author(s). Advanced Materials Technologies published by Wiley-VCH GmbH

2365709x, 2025, 19, Downloaded from https://advanced.onlinelibrary.wiley.com/doi/10.1002/admt.202500090 by Imperial College London, Wiley Online Library on [03/11/2025]. See the Terms and Conditions (https://onlinelibrary.wiley.com/terms-and-conditions) on Wiley Online Library for rules of use; OA articles are governed by the applicable Creative Commons License

Table 1. Chemical compositions of the two green-light photocurable resins used in this work.

Sample	DI Water	$PEGDA_{700}$	AAm	Eosin Y	NVP	TEA
	w/w %			w/w % based on total mass		
$gDLP_{PEGDA}$	55	45	0	0.5	0.5	0.5
$gDLP_{PEGDA/AA}$	40	45	15	0.5	0.5	0.5

Prints were rinsed with DI water prior to imaging and inspection to ensure no excess resin was cured whilst imaging. Blue dye (Dr Oetker Blue food colouring) was diluted in water and injected into the structures to help visualize internal structures. Images were recorded from the microscope using XiCOP software (XIMEA) v4.20 featuring default settings. Data analysis was carried out with ImageJ using the analyze function to set a scale bar and the measure function to calculate the distance between two points.

2.4. Swelling Studies

After completion of the 3D printing, the swelling degree of the hydrogels was evaluated. Excess or uncured resin was removed by rinsing the prints with DI water 5 times in a beaker of 100 mL. The prints of the 3D printed $gDLP_{PEGDA/AA}$ and $gDLP_{PEGDA}$ (exact composition shown in **Table 1**) Solid, Lattice and Hole structures were weighed at time 0 hr and then swollen in DI water at room temperature and after an interval of 48 h weighed again to calculate the swelling ratio for each of the three structures. The swelling ratio was calculated using Equation (1).

$$Swelling(\%) = \frac{M_{s(t)} - M_d}{M_{s(t)}} \quad (1)$$

M_s corresponds to the swollen mass of the sample at a specified time (t) and M_d refers to the dry mass of the sample.

2.5. Mechanical Testing

During the process of sample preparation, removal from the print build plate was carefully carried out using cotton thread, running parallel to the build plate to ensure samples had flat bottom and top surfaces for an even distribution of force during testing. Samples with uneven surfaces were discarded from testing. Prior to testing all samples were post-cured using a LED visible light torch (WUBEN 1200 Lumens) for 10 mins. After washing and post-curing, hydrogels were dried overnight at 60 C before swelling in DI-water for 48 hours. Swollen samples of $gDLP_{PEGDA/AA}$ and $gDLP_{PEGDA}$ Solid, Lattice and Hole were used for mechanical analysis in compression, using a Zwick Roell z2.5 machine fitted with a load cell of 10 kN, and a strain rate of 1.5 mm/min. The machine was operated using Bluehill 3 software (Instron). Five repeats per sample structure (Solid, Hole and Lattice) were tested. Mechanical testing was conducted on all swollen samples until mechanical failure of the material was achieved. Failure of the material was the first sign of fracture whilst under strain.

2.6. Scanning Electron Microscopy (SEM)

Samples of $gDLP_{PEGDA/AA}$ and $gDLP_{PEGDA}$ 3D printed hydrogel were swollen in DI water for 48 hr and then cut into cube shaped pieces (5 mm x 5 mm x 5 mm) to examine cross-sections of their internal structures. The cut samples were placed in a -80 °C freezer overnight to avoid structural collapse during freeze drying. Samples were then freeze dried for 24 hr at – 92 °C. Prior to SEM imaging, freeze dried samples were sputter coated with gold for 2 min at 20 mA to form a 15 nm layer. Next, silver was dissolved in acetone and used to coat one edge of each sample to avoid charging whilst imaging. Samples were imaged using the JEOL 6010LA microscope in secondary electron mode at 8 – 12 kV with a working distance of 8 – 13 mm.

2.7. Optimization Workflow

The overall optimization process is summarized in a workflow shown in **Figure 3**.

The workflow was established to create a common set of steps to achieve printable formulations for DLP printers. The steps are generic and can be applied to any wavelength of light utilized. Specifically, this optimization process aims to achieve scaffolds with porous structures.

3. Results and Discussion

3.1. Optimization of Photoresin for gDLP Printing

A DLP printer as shown in **Figure 4c** was converted to a gDLP and different photoresins were formulated for use in conjunction with a cost-effective, water-soluble photoinitiator, Eosin Y, which exhibits its maximum absorption in the green region of the visible spectrum at a wavelength of 513 nm, as shown Figure 4a,b.

The first step of the optimization workflow (Methods, 3) consisted of a cure speed panel test comprising a series of squares with increasing light durations, ranging from 30 to 100 s with 10 s increments. A maximum limit of 100 s was set to ensure an overall efficient and rapid production of future constructs. A 50 µm FEP film was placed over the LCD screen and a thin layer of photoresin was poured over, as shown in the Appendix A2. The purpose of this test was to determine the effective light duration required to form a consistent, solid layer to ensure a successful 3D printing process. The photoinitiating system consisting of Eosin-Y, TEA and NVP was tested at a range of 0.05 to 0.5 w/w% to find the most effective combination of photoinitiator concentration and light duration as shown in Figure 4. Surface irregularities in the printed hydrogels may stem from multiple factors, including the hydrogel removal process from the build plate, as detailed in the Materials and Methods section. Additional contributors to surface irregularities may have stemmed from oxygen diffusion at the resin-air interface during printing and post-printing swelling in DI water which may magnify pre-existing micro-defects from the removal process. Hydrogels were printed directly onto the build plate without the use of support structures. Given the inherently soft and deformable

© 2025 The Author(s). Advanced Materials Technologies published by Wiley-VCH GmbH

2365709x, 2025, 19, Downloaded from https://advanced.onlinelibrary.wiley.com/doi/10.1002/admt.202500090 by Imperial College London, Wiley Online Library on [03/11/2025]. See the Terms and Conditions (https://onlinelibrary.wiley.com/terms-and-conditions) on Wiley Online Library for rules of use; OA articles are governed by the applicable Creative Commons License

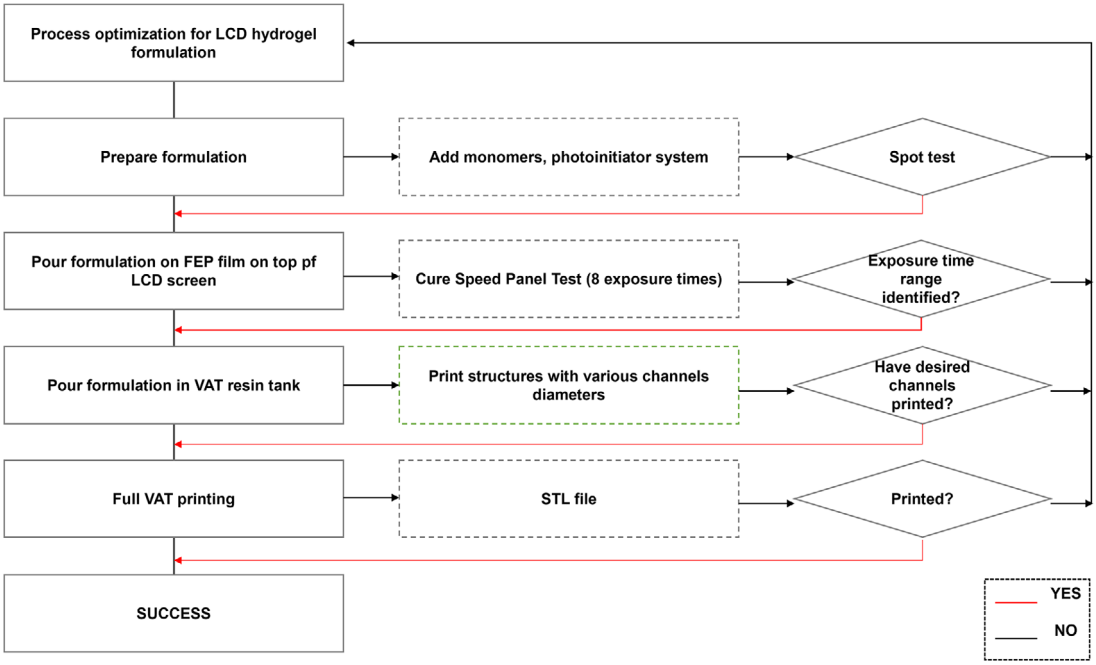


Figure 3. Optimization process for developing a 3D printing formulation specifically for digital light printers (DLP).

nature of hydrogel materials, direct adhesion to the build plate can result in localized stress concentrations and deformation during detachment, contributing to surface and structural defects. To address these defects, future prints may incorporate support structures to better distribute mechanical stress, or be oriented at an angle to reduce contact area and adhesion. Additionally, rounding or filleting base edges can minimize stress concentrations and enable easier, more controlled removal from the build plate.

Unsuccessful gelation was a result of either low exposure times or insufficient monomer and photoinitiator concentrations. Ultimately, the best photoinitiator concentration was found to be 0.5 w/w % with a light duration of 60 s to form a consistent, solid gel layer for both photoresins. However, during a full print cycle, 90 s light duration was used for the first 8 layers to ensure strong adhesion to the build plate, followed by 60 s for the remaining layers. Lower amount of monomers and photoinitiator were also investigated but did not yield any 3D printable formulation within a chosen limit of 100 s per layer exposure time.

After the process of optimization was complete, two final formulations were developed. The typical preparation procedure involved the following steps. Based on a final mass of 100 g, 45 w/w % $PEGDA_{700}$, 15 w/w % AAm and 40 w/w % DI water were mixed in an amber bottle with a magnetic stirrer. Next, based on the total mass of the resin, 0.5 w/w % of TEA and Eosin Y were added, followed by 0.5 w/w % of NVP. The mixture was left to mix for 1 hr before being loaded into the tank. This mixture is referred to as $gDLP_{PEGDA/AA}$. A second photoresin with 0 w/w % AAm (to compare the variation in properties) was synthesized in the same manner and labelled as $gDLP_{PEGDA}$, both formulations are summarized in Table 1.

3.2. Optimizing Layer Exposure Times for Higher Resolution Printing

Following the optimization process workflow from Figure 3, a test artifact with a series of square channels of varying lengths was designed to investigate the optimal light duration required to achieve hollow channels as shown in **Figure 5**. The square design was chosen to avoid any anti-aliasing effects due to the square geometry of the pixels from the LCD screen. Initial tests showed the difference in exposure time from bottom layers (first 8 layers) to normal layers resulted in channel occlusion due to overcuring of the bottom layers. As a result, a taper angle of 3° was used to counter the effect of overcuring due to longer exposure times during the first 8 bottom layers. Slight overcuring can result due to the use of higher exposure times which are needed to provide sufficient interlayer bonding to maintain structural stability. In addition, overcuring on one side of the print could result due to the scattering of the light from the reflective platform which re-cures the photopolymer in the area closer to the platform. The results showed that prints with 50 µm layer heights required light exposure of 60 s to achieve the highest accuracy compared to the CAD design. Figure 5d,e shows the results for normal layer exposure times of 40, 60, and 80 s for $gDLP_{PEGDA/AA}$. For the tested formulations and prints, 0.3 and 0.2 mm channels could not be printed accurately enough to be investigated fully. The minimum channel obtained for $gDLP_{PEGDA/AA}$ was measured to be 0.3 mm obtained with 60 s exposure time which should have corresponded to an intended 0.4 mm channel, indicating slight overcuring.

At the end of optimization the final settings selected for all future prints are displayed in **Table 2**. Figure 5c shows a test artifact injected with blue dye to highlight that the channels are all visible, printed with $gDLP_{PEGDA/AA}$ with light exposure of 60 s for normal layers and 90 s for bottom layers. An optical microscope was also

© 2025 The Author(s). Advanced Materials Technologies published by Wiley-VCH GmbH

2365709x, 2025, 19, Downloaded from https://advanced.onlinelibrary.wiley.com/doi/10.1002/admt.202500090 by Imperial College London, Wiley Online Library on [03/11/2025]. See the Terms and Conditions (https://onlinelibrary.wiley.com/terms-and-conditions) on Wiley Online Library for rules of use; OA articles are governed by the applicable Creative Commons License

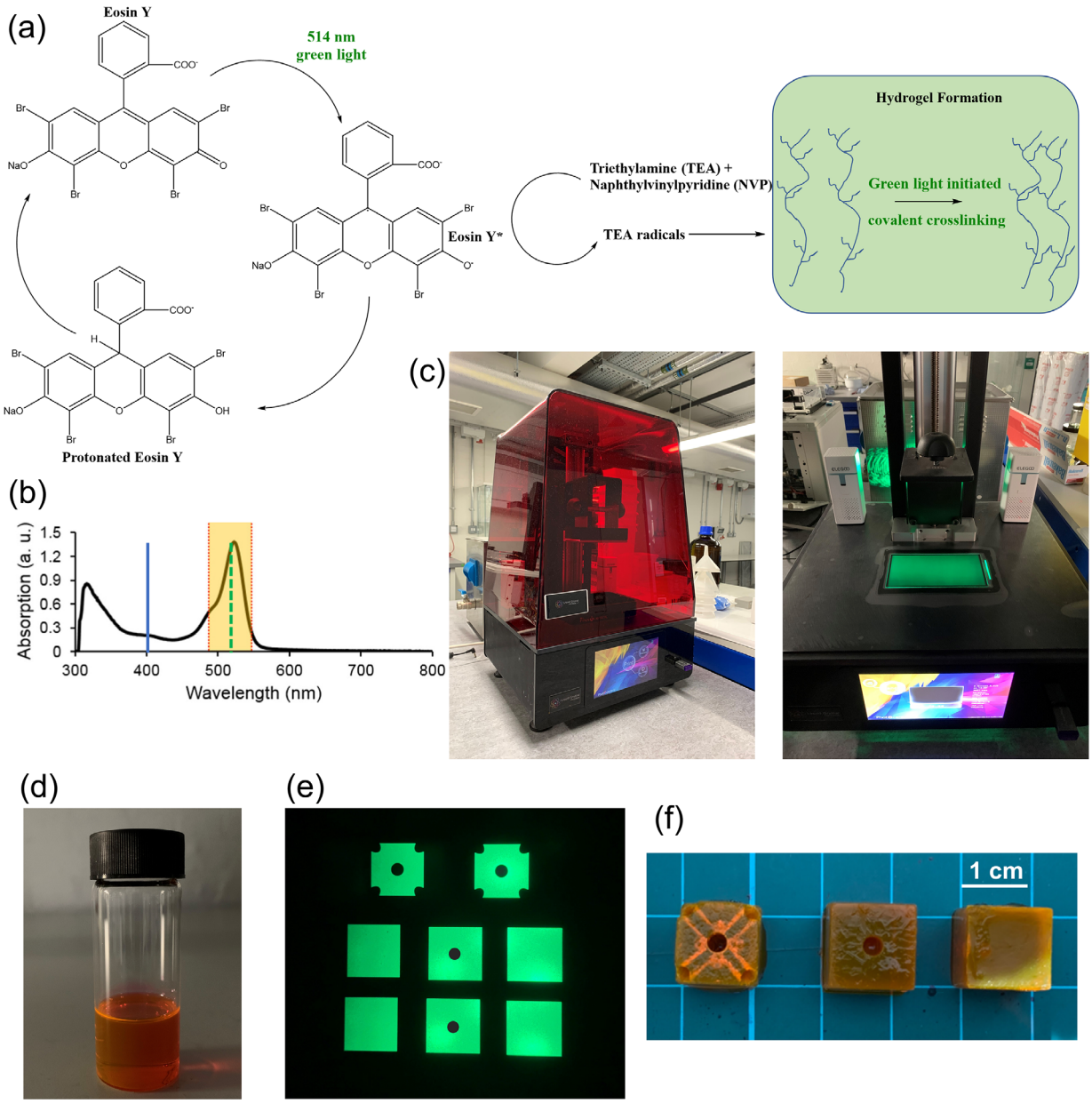


Figure 4. Image displaying Eosin Y-based photopolymerization system. a) A schematic representation of radical generation reactions initiated by photo-induced activation of Eosin Y. b) UV-vis spectra of Eosin Y at pH 7.4. c) gDLP printer (left) and gDLP with green light LEDs on. (d) $gDLP_{PEGDA/AA}$ photoresin sample. e) LCD screen during gDLP print showing Solid, Lattice and Hole structures being printed. f) 3D printed samples of $gDLP_{PEGDA/AA}$ after being washed and post-cured.

used to investigate the layer height accuracy directly after printing. Three separate prints were used, and measurements were taken at different locations (central and the two edges) within the prints surface and averaged out. The final average layer height value was found to be 43.4 ± 0.6 µm for a design layer height of 50 µm. This observed discrepancy in the final average layer height can be attributed to the phenomenon of resin shrinkage occurring during the photopolymerization process.[33] **Figure A3** in the Appendix provides an example of the image used to investigate the layer heights. Similar results were achieved for the photoresin $gDLP_{PEGDA}$.

3.2.1. CAD Design and 3D Printing

Following the optimization process workflow shown in Figure 3 and print optimization process to achieve hollow channels in Figure 5, test artifacts were printed to validate the printing parameters. Test specimens consisted of 1 cm^3 cubes designed using Fusion 360 (Autodesk, USA). The initial designs consisted of a solid cube (Solid), a cube with a single channel (Hole) and a cube with interconnected channels (Lattice) which were printed without the addition of any support structures. The optimized settings used for the $gDLP_{PEGDA}$ solution were an anti-aliasing effect of 8x,

© 2025 The Author(s). Advanced Materials Technologies published by Wiley-VCH GmbH

2365709x, 2025, 19, Downloaded from https://advanced.onlinelibrary.wiley.com/doi/10.1002/admt.202500090 by Imperial College London, Wiley Online Library on [03/11/2025]. See the Terms and Conditions (https://onlinelibrary.wiley.com/terms-and-conditions) on Wiley Online Library for rules of use; OA articles are governed by the applicable Creative Commons License

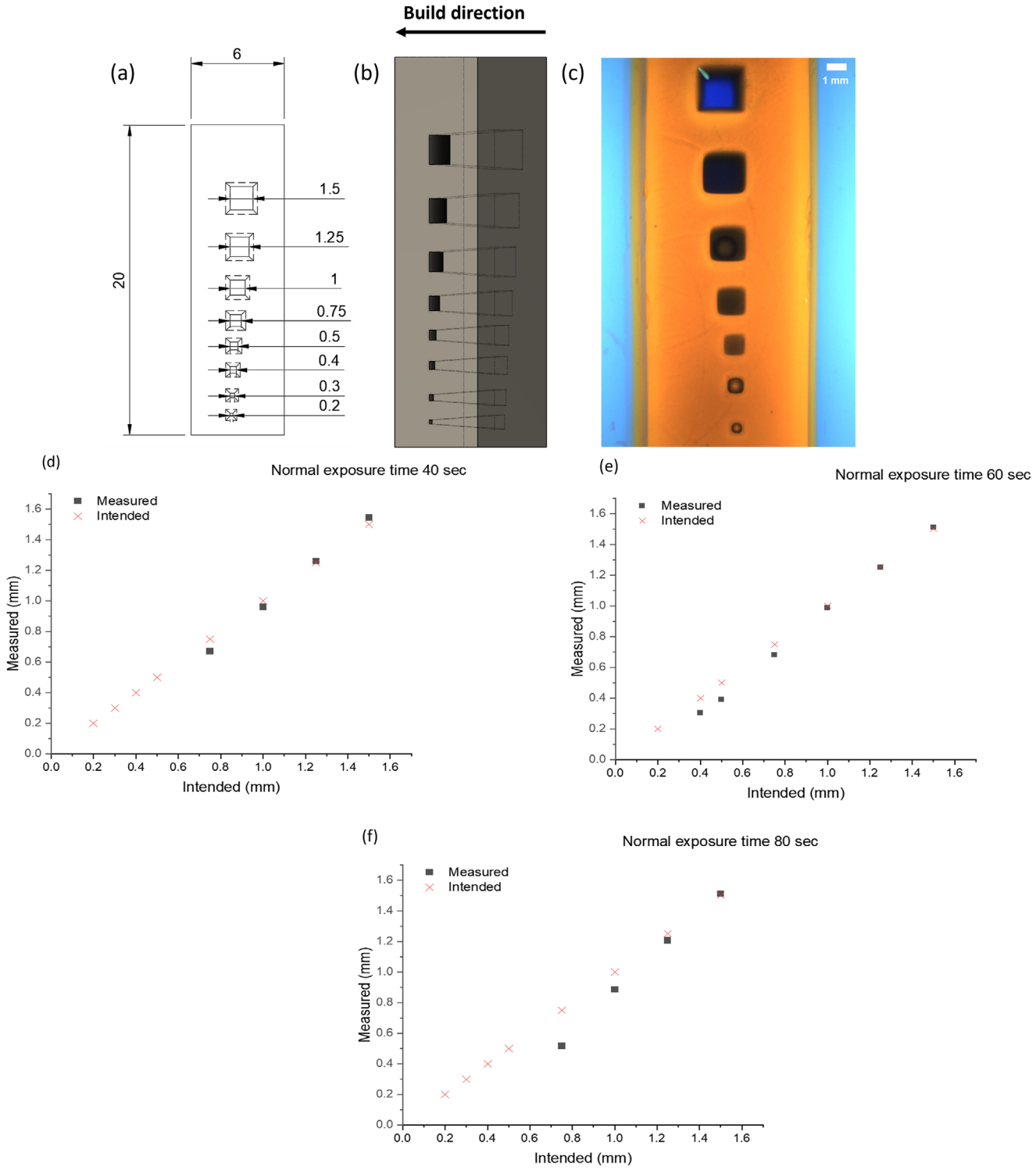


Figure 5. Image representing (a) CAD file specifying the dimensions of the design structure used to study "measured vs. intended" dimensions in mm, (b) image of STL file used for printing with arrow indicating build direction, and (c) 3D printed hydrogel using blue dye for better visualization. Graphs of $gDLP_{PEGDA/AA}$ showing the Measured (3D printed) vs. Intended (CAD) sizes of channels printed using (d) 40 s, (e) 60 s, and (f) 80 s exposure times; the data points are the average of three repeats. Results are most accurate when using a 60 sec exposure time.

© 2025 The Author(s). Advanced Materials Technologies published by Wiley-VCH GmbH

2365709x, 2025, 19, Downloaded from https://advanced.onlinelibrary.wiley.com/doi/10.1002/admt.202500090 by Imperial College London, Wiley Online Library on [03/11/2025]. See the Terms and Conditions (https://onlinelibrary.wiley.com/terms-and-conditions) on Wiley Online Library for rules of use; OA articles are governed by the applicable Creative Commons License

Table 2. gDLP print settings used for the $gDLP_{PEGDA}$ and $gDLP_{PEGDA/AA}$.

Print Settings	
Slice thickness	50 µm
Light power and intensity	0.80 mW, 1.08 mW/ cm^2 (A1)
# Bottom Layers	8
Exposure bottom layers	90000 ms
Z retract speed	100 mm/min
Pixel dimming	0 %
Exposure normal layers	60000 ms
Off time between layers	1000 ms
Z lift distance normal layers	6 mm

a bottom exposure time of for 8 layers and 80 s normal exposure time of 60 s using a layer height of 50 µm. For $gDLP_{PEGDA/AA}$, the same settings were used with an adjusted bottom exposure time of 90 s to ensure adherence to the build plate. The prints are shown in **Figure** 2b–d, demonstrating successful fabrication of all three structures. In particular the lattice structure presents all channels as per design. The successful fabrication of lattice structures using a water-based photo-initiated (PI) system and visible light marks a significant milestone in advancing research for potential applications in visible light printing for biofabrication, low energy excitation polymerization and smart materials. The three designs described were used for further testing including swelling properties and mechanical testing.

3.3. Complex Prints and ASTM Test Files

To further test the ability of the gDLP printer after successfully optimizing the photoresin formulations using the methods from Figure 3 and Figure 5, more complex structures were 3D printed to test the printers capability. 1 cm^3 cubes with a higher density of channels with a reduced diameter size of 1 mm were printed, along with a 6 mm rotary propeller **Figure** 6a,c. Furthermore, to assess the geometric capability of the green light LCD system and benchmark it towards AM standardization, the ASTM/ISO standards were investigated. Test artifacts from the ISO/ASTM 52902:2019 were used to assess geometric errors corresponding to the Resolution slot, Linear artifact and Resolution holes CAD designs were fabricated as shown in Figure 6b,e.[34]

As the goal of the ASTM/ISO tests is to provide an estimated resolution which can be achieved by the AM process under examination, it is expected that not all features present in the CAD design are successfully printed. The designs after printing were thus investigated to obtain more information design consideration that could be taken into account to improve the AM process. The material properties of the hydrogel combined with the small dimensions of the test artifact, resulted in shrinkage post printing ultimately affecting dimensional analysis which can be seen in Figure 6b,d. With regards to the resolution slot test, the spacing between the ribs is visually present, however, due to the reactiveness of the photoresin, a fraction of it may have remained trapped in the slots causing fusing between the parts. An examination of the build file suggests that these features would require less viscous solutions to be successfully fabricated. Failed holes in the case of the Resolution holes artifact, are expected to present signs of printing on the surface but will be solid (i.e., filled) below. Thus, the features beyond the surface were carefully examined by probing the hydrogel with a gauge pin. The results from the Resolution Hole test artifact show diameters of 0.37, 0.26, and 0.16 mm which indicate overcuring. The ideal dimensions would be channels of 0.5, 0.4, 0.3, 0.2, and 0.1 mm diameter. Overcuring in water-based hydrogels can occur if residual unreacted photopolymer resin remains after rinsing, which can diffuse to the surface over time. When the hydrogel is analyzed under an optical microscope, the light used for imaging may inadvertently activate this residual resin, leading to localized overcuring. In addition, not including taper angles could also contribute to overcuring due to the longer bottom exposure times required for stronger build plate adhesion. In relation to the Linear test artifact (Figure 6) the ideal spacing between the prismatic protrusions is expected to be increasing from 5 mm to 7.5 mm, 10 mm, and 12.5 cm. The percentage deviation between the measured distances and the ideal ones is of –10 %, meaning measured distances are shorter than ideal ones. This effect can be caused by both material warping and overcuring. Warping can result from residual stress but also due to thin bounding box around the ASTM/ISO tests which measure 3 mm in length, facilitating material warping due to the hydrated nature of the material. The tests suggest that water based photoresins require different or improved ISO standards to account for the presence of water in the material. The ASTM tests were performed on both developed formulations resulting in similar results.

Finally, to demonstrate the capability of the developed system to achieve complex structures, the highest vascular structure printable, a 1 cm^3 consisting of 8 x 0.5 cm^3 7-strut lattice cubes with 1 mm diameter channels were designed and 3D printed, shown in Figure 6a. The print demonstrates the ability of the gDLP printer to create complex hydrogel geometries with features present from the cm to the µm range which is currently not possible to achieve through conventional manufacturing (e.g., moulding). The proposed optimization process for developing 3D printing formulations for the gDLP showcases the ability to formulate photoresins with complex geometries. In addition, the workflow presented can extended for the optimization of any DLP printer where different wavelengths could be further explored to increase the efficiency of the printing process and achieve higher resolutions structures.

3.4. Swelling Studies

The printed hydrogels were soaked in water for 48 hr to calculate the swelling ratio and examine the impact of hydrostatic pressures on the structural integrity of the prints. The results indicate that the $gDLP_{PEGDA/AA}$ formulation had the highest swelling ratio with a value of 39.52 %, followed by 25.80 % for the $gDLP_{PEGDA}$ formulation. For both formulations, the lattice exhibited the highest swelling rate value. Water uptake is greater for the lattice structures due to larger surface areas and more entry points for water to diffuse through the hydrogels. The result indicates that the hydrophilic nature of AAm leads to an increased swelling ratio relative to $PEGDA_{700}$ on its own. Finally, all prints retained their structure after swelling, with channels increasing slightly in

© 2025 The Author(s). Advanced Materials Technologies published by Wiley-VCH GmbH

2365709x, 2025, 19, Downloaded from https://advanced.onlinelibrary.wiley.com/doi/10.1002/admt.202500090 by Imperial College London, Wiley Online Library on [03/11/2025]. See the Terms and Conditions (https://onlinelibrary.wiley.com/terms-and-conditions) on Wiley Online Library for rules of use; OA articles are governed by the applicable Creative Commons License

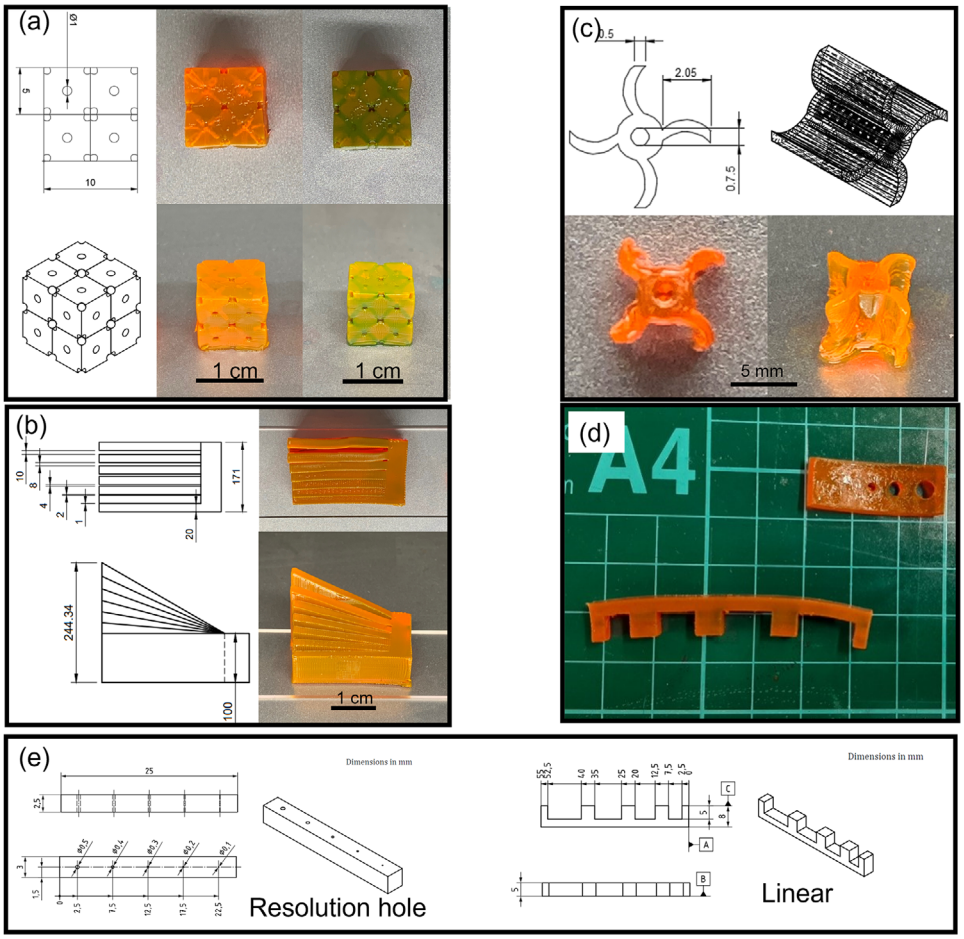


Figure 6. A comparison of 3D prints using the developed photoresin and their respective CAD designs. (a) A 1 cm^3 cube with a highly connected 1 mm diameter lattice network, before and after blue dye infusion, (b) an ASTM resolution slot test (ISO/ASTM 52902/2019) with varying dimensions and gaps between arms, showing all parts successfully printed, and (c) a 6 mm rotary propeller (d) a printed linear and resolution hole test (e) An ASTM linear and resolution hole test (ISO/ASTM 52902/2019). All CAD dimensions are in given in mm.

diameter as a result of water uptake. The mechanical integrity of the prints was sustained without any visible damage or breakage during water uptake. The results of the compressive and swelling studies are displayed in **Figure 7**. These results signify the initial progress in developing hydrophilic structures capable of providing solid anchorage to support life even in a swollen state.

3.5. Mechanical Testing

Material properties were then characterised in terms of mechanical compression tests of the 3D printed hydrogels. Both $gDLP_{PEGDA}$ and $gDLP_{PEGDA/AA}$ were investigated under compression. Figure 7a shows an example of the set up used to test the printed samples and Figure 7b shows the compressed print after mechanical failure. Figure 7c,d summarize the average compressive stress for applications in Solid, Hole and Lattice prints of $gDLP_{PEGDA/AA}$ and $gDLP_{PEGDA}$, respectively. Figure 7c,d provides an example of the applications in Solid, Hole and Lattice compressive profiles of $gDLP_{PEGDA/AA}$ and $gDLP_{PEGDA}$, respectively. The results evidence a major difference in compressive strength as a result of the addition of AAm in the formulation. The presence of a second network in the hydrogel structure could be creating crosslinking points between the first and second network which has already been observed in previous findings.[35] This would promote energy dissipation and stress under loading increasing the compressive strength of the overall structure.

The compressive profiles indicate that reducing the solid density of the print by incorporating a connected lattice structure lowers the stress-to-strain response, as shown in Figure 7e,f. The Hole design with a single central channel experienced both a reduced compressive strength and strain for $gDLP_{PEGDA/AA}$ samples as density of the design was reduced i.e., Solid to Lattice. However, $gDLP_{PEGDA}$ samples only experienced a reduced compressive strain with increased design complexity, whilst strain values increased. This is likely due to the higher stiffness experienced by $gDLP_{PEGDA/AA}$ samples compared to $gDLP_{PEGDA}$. Ultimately, the lattice structure exhibits the lowest compressive stress value due to the increased number of failure points inherent in its design. In addition, the lattice structure exhibits the highest swelling ratio. Since the mechanical tests were conducted

© 2025 The Author(s). Advanced Materials Technologies published by Wiley-VCH GmbH

2365709x, 2025, 19, Downloaded from https://advanced.onlinelibrary.wiley.com/doi/10.1002/admt.202500090 by Imperial College London, Wiley Online Library on [03/11/2025]. See the Terms and Conditions (https://onlinelibrary.wiley.com/terms-and-conditions) on Wiley Online Library for rules of use; OA articles are governed by the applicable Creative Commons License

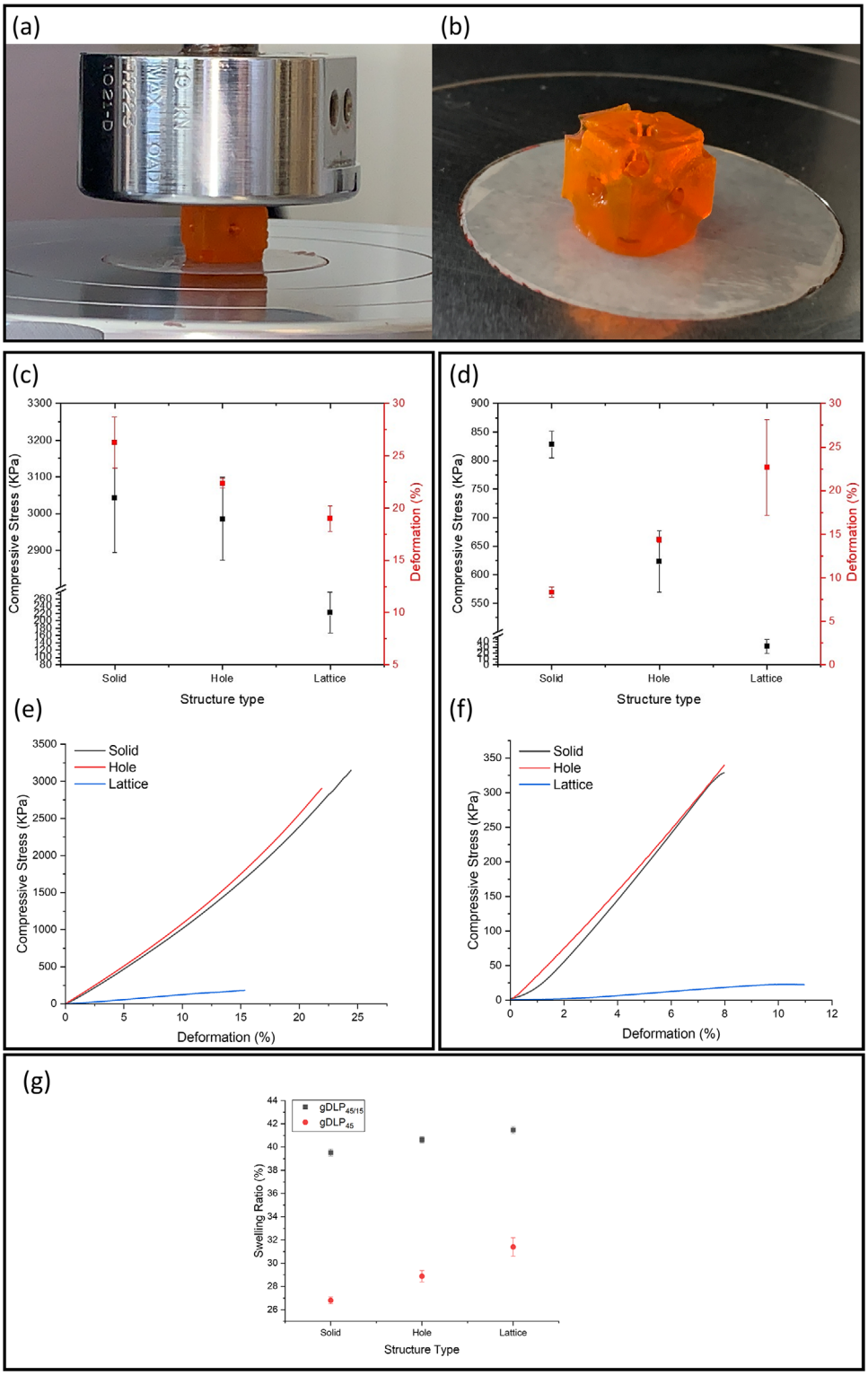


Figure 7. a) Compressive tests performed on gDLP45/15 showing compression of a Lattice print, b) fractured Lattice print post-compression. c) Compressive tests performed on Solid, Hole and Lattice structures of $gDLP_{PEGDA/AA}$. d) Compressive tests performed on Solid, hole and lattice structures of $gDLP_{PEGDA}$. Error bars indicate standard deviations. g) Swelling ratio of $gDLP_{PEGDA/AA}$ and $gDLP_{PEGDA}$ prints for Solid, Hole and Lattice structures. Error bars indicate standard deviation.

© 2025 The Author(s). Advanced Materials Technologies published by Wiley-VCH GmbH

2365709x, 2025, 19, Downloaded from https://advanced.onlinelibrary.wiley.com/doi/10.1002/admt.202500090 by Imperial College London, Wiley Online Library on [03/11/2025]. See the Terms and Conditions (https://onlinelibrary.wiley.com/terms-and-conditions) on Wiley Online Library for rules of use; OA articles are governed by the applicable Creative Commons License

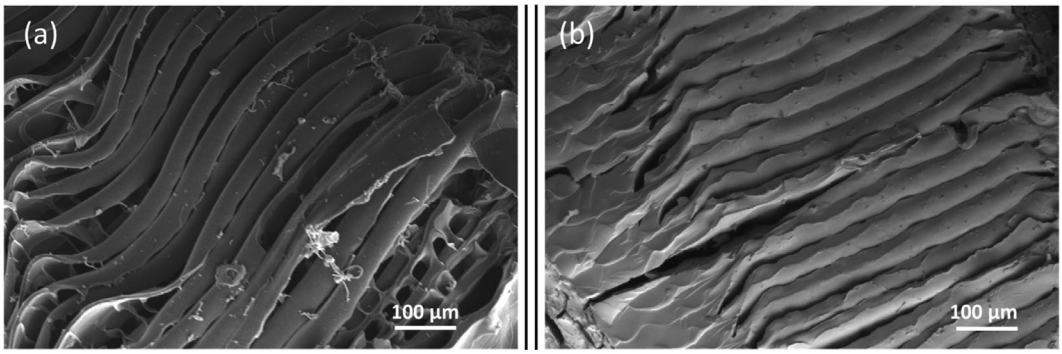


Figure 8. SEM analysis of vertical section on 3D printed solid hydrogels for (a) $gDLP_{PEGDA}$ and (b) $gDLP_{PEGDA/AA}$.

on hydrated samples, the higher water content present in the lattice structure contributed to the reduction of the compressive strength. The results demonstrate the possibility to use green light DLP printing to fabricate robust structures with varied mechanical properties that overcome the typical limitation of MEX printing highlighted in the introduction.

3.6. SEM

SEM imaging was performed on the two formulations to investigate the layer structures of the 3D printed hydrogels. The samples were swollen for 48 hr and freeze dried prior to imaging. **Figure 8** shows a compact structure for both $gDLP_{PEGDA}$ and $gDLP_{PEGDA/AA}$ with 3D printed layers clearly displayed of a thickness of ca 50 µm corresponding to the layer thickness used in the fabrication process. The SEM image of the $gDLP_{PEGDA}$ shows that the layers begin to unravel compared to $gDLP_{PEGDA/AA}$, due to weaker interlayer bonding and possibly due to the lower mechanical strength as reflected in the compressive tests. This could occur during the freeze-drying process, where the polymer network shrinks and thereby causing layer delamination. This did not occur in the $gDLP_{PEGDA/AA}$ prints. The $gDLP_{PEGDA/AA}$ sample does not present any evident signs of pore interconnectivity and the layers are tighter due to crosslinking between PEGDA and AAm compared to $gDLP_{PEGDA}$. SEM analysis also revealed that the printed hydrogels were not as porous as 3D printed hydrogels using a commercial SLA.[36] This effect could be caused by the inherent difference between the two fabrication methods used, whereby an SLA curing point by point could lead to micrograps formation compared to a more uniform curing due to an entire layer of photoresin being formed such as in a DLP. The layer by layer fashion of curing could also result in stronger interlayer adhesion compared to the SLA. A further reason could be found in the differences in water percentage used in the study, the SLA formulation compared to the gDLP one had a higher percentage of water which combined to the localised heat of the laser source could result in phase separation within the resin and hence the formation of pores. Therefore, the fabrication of a layer in a single exposure typical of a DLP shows a superior capability to printing structures with uniform weights and dimensions. Similar results were found in previous research where 20 w/v % PEGDA tablets were printed using a commercial DLP.[37]

4. Conclusion

To our knowledge, this work pioneers the green-light DLP printing of high-resolution (50 µm), water-rich hydrogels (60 % water) with complex geometries, enabled by a cost-effective, water-soluble formulation and scalable, converted commercial hardware. A workflow for formulating photoresins suitable for gDLP printing has been presented, offering valuable resources to the scientific community for use in various formulation development efforts. ASTM/ISO standards were investigated to benchmark the developed resins evidencing the need for novel standards aimed at water based formulations. The addition of AAm in the formulation did not significantly affect achievable resolution but did lead to an increase in the swelling ratio and compressive strength. This study lays the groundwork for further advancements in the field, offering promising prospects for applications in tissue engineering, soilless cultivation, and portable printing solutions that can greatly benefit from green light 3D printing. The technique may bring advancements in the fields of bioprinting and biofabrication, as well as in-situ living organism printing, with green light Vat-Photopolymerisation providing a more biocompatible process due to the use of visible light and the availability of cost-effective water-soluble photoinitiators. The 3D printed hydrogels presented in this study have exhibited customizable mechanical properties and swelling behaviors, as well as the capability to create complex structures using water-based formulations. Future investigations are needed to assess the feasibility of 3D printing with live cells or microorganisms. To enhance the appeal of this fabrication technique, optimizations in the chemical formulation, including the photoinitiating system, stimuli-responsive particles, and additives like oxygen scavengers, will be essential to reduce layer exposure times. Furthermore, on the hardware front, more efficient optical systems, such as LCDs, should be subject to further research to improve light transmission.

Appendix A

A.1

Measured power output of customized gDLP in comparison to a commercial DLP printer.

An example of models to optimize channel printing and minimize overcuring during fabrication shown in Figure A3.

© 2025 The Author(s). Advanced Materials Technologies published by Wiley-VCH GmbH

2365709x, 2025, 19, Downloaded from https://advanced.onlinelibrary.wiley.com/doi/10.1002/admt.202500090 by Imperial College London, Wiley Online Library on [03/11/2025]. See the Terms and Conditions (https://onlinelibrary.wiley.com/terms-and-conditions) on Wiley Online Library for rules of use; OA articles are governed by the applicable Creative Commons License

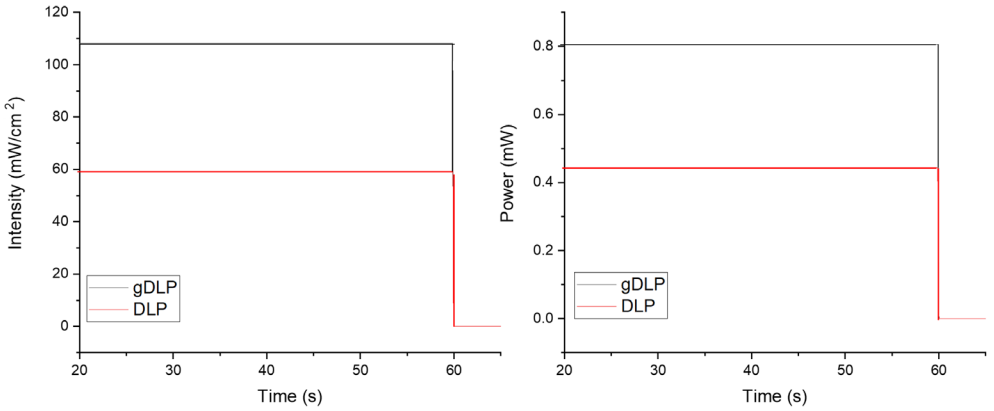


Figure A1. Intensity (mW/cm^2) and Power output (mW) of the gDLP (black line) relative to a commercial DLP (red line) printer during a 60 s test.

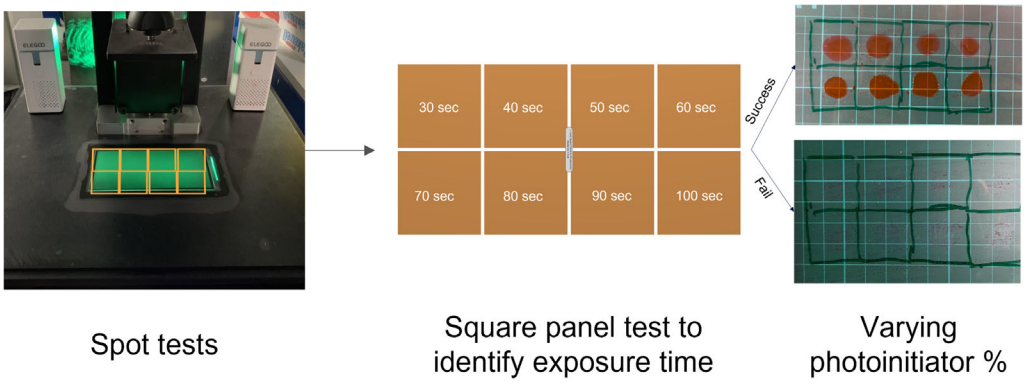


Figure A2. Square panel method for identifying exposure time on with different photoinitiating system and photoresin components.

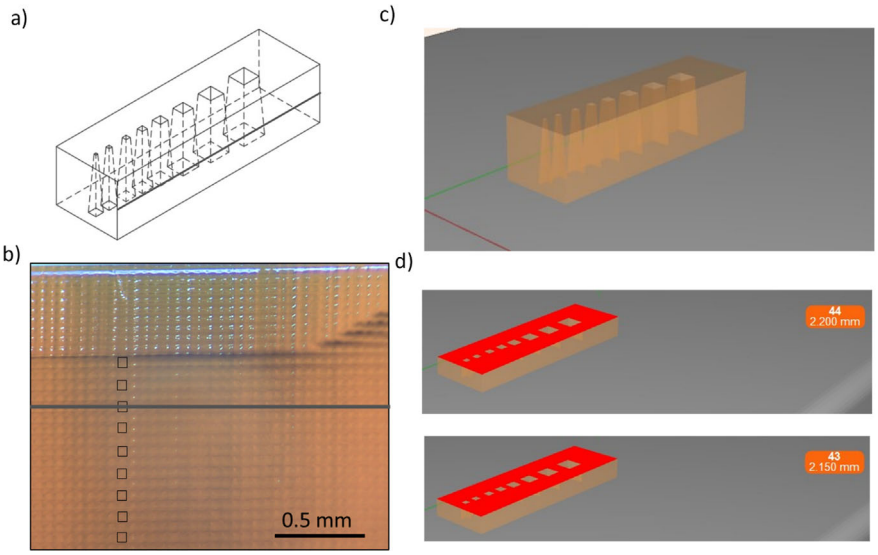


Figure A3. A gDLP$_{PEGDA/AA}$ CAD design of square channels (a) and the resulting print under an optical microscope clearly showing layers formation (b). The CAD design was imported into Photocentric Studio (c) using a print profile of 50 µm (d). The line drawn in (a) is shown for representing a virtual layer as reported in (b).

© 2025 The Author(s). Advanced Materials Technologies published by Wiley-VCH GmbH

2365709x, 2025, 19, Downloaded from https://advanced.onlinelibrary.wiley.com/doi/10.1002/admt.202500090 by Imperial College London, Wiley Online Library on [03/11/2025]. See the Terms and Conditions (https://onlinelibrary.wiley.com/terms-and-conditions) on Wiley Online Library for rules of use; OA articles are governed by the applicable Creative Commons License

Acknowledgements

The authors would like to thank Dr. Mark Friddin from Imperial College London for his support on the optical microscope. In addition, the authors would like to thank Photocentric ltd and Roberto Angelini for their technical support on the hardware of the printer. Finally the authors would like to thank Borut Lampret for testing the power output and intensity of the gDLP and DLP printers. This work was supported by The Leverhulme Trust's 'Leverhulme Doctoral Scholarship Programme' and the Engineering and Physical Research Council (Grant Number: EP/L015498/1). Further funding resulted from the Imperial College London President's Excellence Fund for Frontier Research and from Imperial College London Undergraduate Research Opportunities Programme.

Conflict of Interest

The authors declare no conflict of interest.

Author Contributions

Conceptualization, L.M.Kalossaka; methodology, L.M,Kalossaka; validation, L.M.Kalossaka, A.A.Mohammed, L.Bastos; investigation, L.M.Kalossaka; writing—original draft preparation, L.M.Kalossaka, A.A.Mohammed; writing—review and editing, L.M.Kalossaka, A.A.Mohammed; visualization, L.M.Kalossaka, A.A.Mohammed.; supervision, L.Barter, C.Myant.

Data Availability Statement

The data that support the findings of this study are available from the corresponding author upon reasonable request.

Keywords

biofabrication, hydrogels, laser-based AM processes, lattice structures

Received: January 14, 2025
Revised: May 2, 2025
Published online: July 1, 2025

[1] M. R. Hartings, Z. Ahmed, *Nat. Rev. Chem.* **2019**, *3*, 305.
[2] J. Borrello, P. Nasser, J. C. Iatridis, K. D. Costa, *Addit. Manuf.* **2018**, *23*, 374.
[3] Y. S. Zhang, A. Khademhosseini, *Science* **2017**, *356*, 6337.
[4] N. Chirani, L. Yahia, L. Gritsch, F. L. Motta, S. Chirani, S. Fare, *J. Biomed. Sci.* **2015**, *4*, 2.
[5] A. Jayakumar, V. K. Jose, J.-M. Lee, *Small Methods* **2020**, *4*, 1900735.
[6] M. Bahraminasab, *Biomed. Eng. Online* **2020**, *19*, 1.
[7] C. Zuppinger, *Front. Cardiovasc. Med.* **2019**, *6*, 87.
[8] L. Kalossaka, Ph.D. Thesis, Imperial College London, **2022**.
[9] M. R. Binelli, A. Kan, L. E. Rozas, G. Pisaturo, N. Prakash, A. R. Studart, *Adv. Mater.* **2023**, *35*, 2207483.
[10] K. C. Hribar, P. Soman, J. Warner, P. Chung, S. Chen, *Lab Chip* **2014**, *14*, 268.
[11] D. Wangpraseurt, S. You, Y. Sun, S. Chen, *Trends Biotechnol.* **2022**, *40*, 843.
[12] L. M. Kalossaka, G. Sena, L. M. Barter, C. Myant, *Appl. Mater. Today* **2021**, *24*, 101088.
[13] R. Levato, T. Jungst, R. G. Scheuring, T. Blunk, J. Groll, J. Malda, *Adv. Mater.* **2020**, *32*, 1906423.
[14] D. Chimene, K. K. Lennox, R. R. Kaunas, A. K. Gaharwar, *Ann. Biomed. Eng.* **2016**, *44*, 2090.
[15] W. E. Hennink, C. F. van Nostrum, *Adv. Drug Delivery Rev.* **2012**, *64*, 223.
[16] C. A. Murphy, K. S. Lim, T. B. Woodfield, *Adv. Mater.* **2022**, *34*, 2107759.
[17] S. Vanaei, M. Parizi, F. Salemizadehparizi, H. Vanaei, *Engineered Regeneration* **2021**, *2*, 1.
[18] S. V. Murphy, A. Atala, *Nat. Biotechnol.* **2014**, *32*, 773.
[19] Z. Wang, R. Abdulla, B. Parker, R. Samanipour, S. Ghosh, K. Kim, *Biofabrication* **2015**, *7*, 045009.
[20] M. Chen, M. Zhong, J. A. Johnson, *Chem. Rev.* **2016**, *116*, 10167.
[21] D. Loterie, P. Delrot, C. Moser, *Nat. Commun.* **2020**, *11*, 1.
[22] A. Bagheri, J. Jin, *ACS Appl. Polym. Mater* **2019**, *1*, 593.
[23] T. Billiet, M. Vandenhaute, J. Schelfhout, S. Van Vlierberghe, P. Dubruel, *Biomaterials* **2012**, *33*, 6020.
[24] W. L. Ng, J. M. Lee, M. Zhou, Y.-W. Chen, K.-X. A. Lee, W. Y. Yeong, Y.-F. Shen, *Biofabrication* **2020**, *12*, 022001.
[25] W. Li, M. Wang, L. S. Mille, J. A. Robledo Lara, V. Huerta, T. Uribe Velázquez, F. Cheng, H. Li, J. Gong, T. Ching, C. A. Murphy, A. Lesha, S. Hassan, T. B. F. Woodfield, K. S. Lim, Y. S. Zhang, *Adv. Mater.* **2021**, *33*, 2102153.
[26] Y. Bao, *Macromol. Rapid Commun.* **2022**, *43*, 2200202.
[27] A. Stafford, D. Ahn, E. K. Raulerson, K.-Y. Chung, K. Sun, D. M. Cadena, E. M. Forrister, S. R. Yost, S. T. Roberts, Z. A. Page, *J. Am. Chem. Soc.* **2020**, *142*, 14733.
[28] P. Chansoria, R. Rizzo, D. Rutsche, H. Liu, P. Delrot, M. Zenobi-Wong, *Chem. Rev.* **2024**, *124*, 8787.
[29] D. Ahn, L. M. Stevens, K. Zhou, Z. A. Page, *ACS Cent. Sci.* **2020**, *6*, 1555.
[30] K. Sun, Y. Zhang, D. Zhu, X. Peng, J. Zhang, T. Gong, M. Ma, P. Xiao, *J. Photochem. Photobiol., C* **2023**, *57*, 100637.
[31] Y. Wu, Y. Zeng, Y. Chen, C. Li, R. Qiu, W. Liu, *Adv. Funct. Mater.* **2021**, *31*, 2107202.
[32] B. Baroli, *J. Pharm. Sci.* **2007**, *96*, 2197.
[33] Q. Zhang, S. Weng, C. M. Hamel, S. M. Montgomery, J. Wu, X. Kuang, K. Zhou, H. J. Qi, *Extreme Mech. Lett.* **2021**, *48*, 101403.
[34] J. Berez, M. Praniewicz, C. Saldana, *Procedia Manuf.* **2021**, *53*, 395.
[35] L. Wang, G. Shan, P. Pan, *Soft Matter* **2014**, *10*, 3850.
[36] L. M. Kalossaka, A. A. Mohammed, G. Sena, L. Barter, C. Myant, *J. Mater. Res.* **2021**, *36*, 4249.
[37] H. Kadry, S. Wadnap, C. Xu, F. Ahsan, *Eur. J. Pharm. Sci.* **2019**, *135*, 60.

© 2025 The Author(s). Advanced Materials Technologies published by Wiley-VCH GmbH

2365709x, 2025, 19, Downloaded from https://advanced.onlinelibrary.wiley.com/doi/10.1002/admt.202500090 by Imperial College London, Wiley Online Library on [03/11/2025]. See the Terms and Conditions (https://onlinelibrary.wiley.com/terms-and-conditions) on Wiley Online Library for rules of use; OA articles are governed by the applicable Creative Commons License